Principal Component Analysis Based on Wavelet Characteristics Applied to Automated Surface Defect Inspection

HONG-DAR LIN[1], CHUNG-YU CHUNG[1], WAN-TING LIN[2]

[1]Department of Industrial Engineering and Management
Chaoyang University of Technology
168 Jifong E. Rd., Wufong Township, Taichung County, 41349
TAIWAN
hdlin@cyut.edu.tw

[2]College of Business, University of Missouri-Columbia
213 Cornell Hall, Columbia, MO 65211
USA

Abstract: - Automated visual inspection, a crucial manufacturing step, has been replacing the more time-consuming and less accurate human inspection. This research explores automated visual inspection of surface defects in a light-emitting diode (LED) chip. Commonly found on chip surface are water-spot blemishes which impair the appearance and functionality of LEDs. Automated inspection of water-spot defects is difficult because they have a semi-opaque appearance and a low intensity contrast with the rough exterior of the LED chip. Moreover, the defect may fall across two different background textures, which further increases detection difficulties. The one-level Haar wavelet transform is first used to decompose a chip image and extract four wavelet characteristics. Then, wavelet-based principal component analysis (WPCA) and Hotelling statistic (WHS) approaches are respectively applied to integrate the multiple wavelet characteristics. Finally, the principal component analysis of WPCA and the Hotelling control limit of WHS individually judge the existence of defects. Experimental results show that the proposed WPCA method achieves detection rates of above 93.8% and false alarm rates of below 3.6%, and outperforms other methods. A valid computer-aided visual defect inspection system is contributed to help meet the quality control needs of LED chip manufacturers.

Key-Words: - Surface defect inspection, Wavelet characteristics, Principal component analysis, Hotelling statistic, Machine vision system.

1 Introduction

Quality control is designed to prevent defective products from reaching the customer. Visual inspection constitutes an important part of quality control in the industry [1-2]. In most cases, quality control through visual inspection is still conducted by humans. However, difficulties exist in detecting defects by human eyes because inspectors are very likely to make erroneous judgments due to personal subjectivity or eye fatigues. Visual inspection determines product properties using visual information and is most often automated by employing machine vision techniques. Therefore, automated visual inspection of surface defects has become a critical task for manufacturers who strive to improve product quality and production efficiency [3-7]. In this study, we use machine vision techniques for automated surface inspection of light-emitting diode (LED) chips.

LED is a semiconductor device that emits visible light when an electric current passes through the semiconductor chip. Compared with incandescent and fluorescent illuminating devices, LEDs have lower power requirement, higher efficiency, and longer lifetime. Typical applications of LED components include indicator lights, LCD panel backlighting, fiber optic data transmission, etc. The basic structure of an LED consists of the light emitting semiconductor chip, a lead frame where the chip is actually placed, and the encapsulation epoxy which surrounds and protects the chip. Figure 1 shows the LED product and basic LED structure diagram. To meet consumer and industry needs, LED products are being made in smaller sizes, which increase difficulties of product inspection.

With the popularity of LEDs, inspection of surface defects has become a critical task for manufacturers who strive to enhance LED product quality. Surface defects affect not only the appearances of LEDs but also their functionality, efficiency and stability. As inspecting surface defects by human eyes is ineffective and inefficient, this

ISSN: 1991-8755 Issue 4, Volume 3, April 2008

research aims to develop an automated vision system for detecting water-spot defects, which commonly appear on the surfaces of LED chips owing to the steam generated during the production process. Automated inspection of a water-spot defect is difficult because the blemish has a semi-opaque appearance and a low intensity contrast with the rough exterior of the LED chip. With a width of 0.21*mm*, an LED chip comprises an aluminum-pad (bonding pad) in the central area and a metal oxide semiconductor (emitting area) in the outer area, as shown in Fig. 2 (a). Texture of the central area has a random pattern while that of the outer area has a uniform appearance. A water-spot blemish may fall across the two areas of significantly different textures, which complicates the defect detection procedure. Figures 2 (b)-(d) display the LED chip images with water-spot blemishes of different shapes.

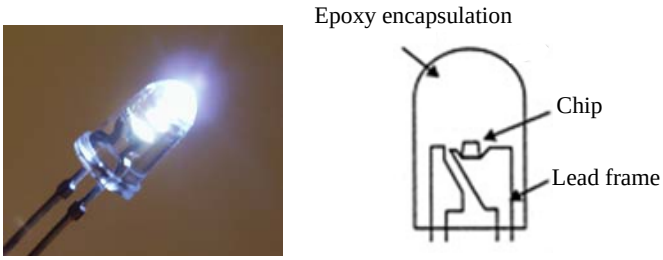

Fig. 1 (a) LED product (b) LED structure diagram

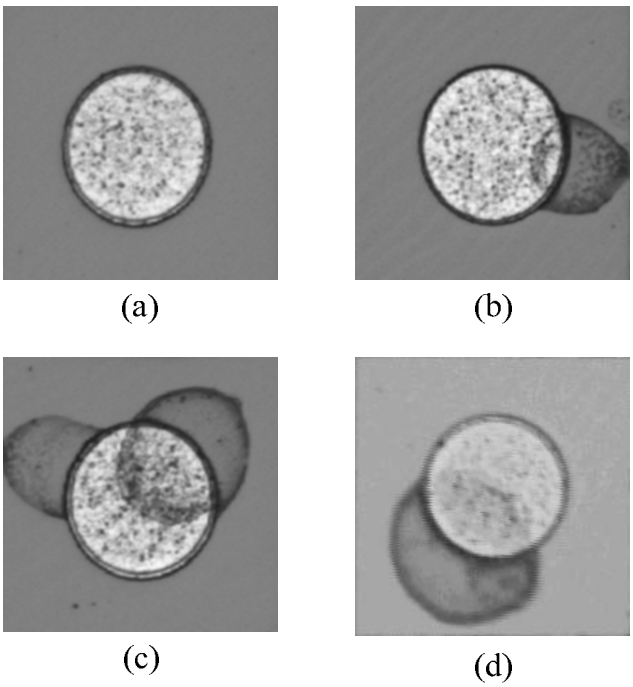

Fig. 2 LED chip images (a) normal chip (b)-(d) defective chips with water-spot defects of different shapes

Defect detection techniques compute a set of textural features in a sliding window and search for significant local deviations among the feature values. The detection techniques are generally classified into the spatial domain and the frequency domain. Siew et al. [8] applied the co-occurrence matrix method, a traditional spatial domain technique, to assess carpet wear by using two-order gray level statistics to build up probability density functions of intensity changes. For another spatial domain example, Latif-Amet et al. [9] presented wavelet theory and co-occurrence matrices for detection of defects encountered in textile images and classified each sub-window as defective or non-defective with a Mahalanobis distance.

As to techniques in the frequency domain, Chan and Pang [10] proposed a simulated fabric model based on Fourier transform for inspection of structural defects in fabric. Since a three-dimensional frequency spectrum is very difficult to analyze and defects occur mostly along the horizontal and vertical axes, the central spatial frequency spectrum approach has been proposed to increase efficiency of the analysis process. Seven significant characteristic parameters can be extracted from the central frequency spectrums for describing the defect types. Kumar and Pang [11] presented a new multi-channel filtering scheme for unsupervised fabric defect detection using a class of self-similar Gabor functions. Also, Lin [12] developed a novel approach that applies discrete cosine transform decomposition and cumulative sum techniques for the detection of tiny defects on passive component chips.

Regarding defect detection applications in the electronic industry, Lin and Chiu [13] used multivariate Hotelling T^2 statistic to integrate different coordinates of color models for MURA-type defect detection on Liquid Crystal Displays (LCD), and applied ant colony algorithm and back-propagation neural network techniques to develop an automatic inspection procedure. Lu and Tsai [14] proposed a global approach for automatic visual inspection of micro defects such as pinholes, scratches, particles and fingerprints. The Singular Value Decomposition (SVD) adopted by Lu and Tsai suits the need for detecting defects on the TFT-LCD images of highly periodical textural structures. Furthermore, in the recent decade, many vision systems have been developed for the inspection of surface defects on semiconductor wafers [15-17]. For instance, Fadzil and Weng [18] implemented a vision inspection system that achieves a 90% probability of accurately classifying defects, scratches,

contamination, blemishes, off center defects, etc. in the encapsulations of diffused LED products.

The aforementioned techniques perform well in anomaly detection, but most of them do not detect defects with the properties of water-spot defects. This research has been motivated by the need for an efficient and effective technique that detects semi-opaque and low-intensity-contrast water-spot defects falling across two different background textures.

2 Proposed Methods

To detect water-spot defects of LED chips, this research adopts the one-level Haar wavelet transform to conduct image transformation and extract wavelet characteristics. We apply the wavelet-based multivariate statistical approaches to integrate multiple wavelet characteristics and then develop the principal component analysis and Hotelling control procedure to individually judge the existence of water-spot defects in LED chip images.

2.1 Wavelet characteristics

The Haar wavelet transform is one of the simplest and basic transformations. Its base transform in the multiple-level scaling space can be implemented as:

$$v_{j,k} = \frac{v_{j+1,2k} + v_{j+1,2k+1}}{2}; w_{j,k} = \frac{v_{j+1,2k} - v_{j+1,2k+1}}{2}. \quad (1)$$

In this research, we apply a standard decomposition that covers wavelet row and column transfers to do the wavelet transform of a two-dimensional image. The Haar transform can be computed stepwise by the mean value and half of the differences of the tristimulus values of two contiguous pixels. We perform the 2-D wavelet transform by applying 1-D wavelet transform first on rows and then on columns. Based on the transfer concept of the one-dimensional space, the Haar wavelet transform can process a two-dimensional image of (M x N) pixels in the following way:

Row transfer:

$$\begin{cases} g_R(p,q) = \left[\frac{g(p,2q) + g(p,2q+1)}{2}\right], \\ g_R(p, q+\left[\frac{N}{2}\right]) = \left[\frac{g(p,2q) - g(p,2q+1)}{2}\right], \\ where\ 0 \le p \le (M-1), 0 \le q \le \left[\frac{N}{2}\right] - 1, [\,]\ is\ Gauss\ symbol. \end{cases} \quad (2)$$

Column transfer:

$$\begin{cases} g_C(p,q) = \left[\frac{g_R(2p,q) + g_R(2p+1,q)}{2}\right], \\ g_C(p+\left[\frac{M}{2}\right], q) = \left[\frac{g_R(2p,q) - g_R(2p+1,q)}{2}\right], \\ where\ 0 \le p \le \left[\frac{M}{2}\right] - 1, 0 \le q \le (N-1). \end{cases} \quad (3)$$

In the above expressions (Eqs. (2)-(3)), $g(p,q)$ represents an original image, $g_R(p,q)$ the row transfer function of $g(p,q)$, and $g_C(p,q)$ the column transfer function of $g_R(p,q)$. As $g_C(p,q)$ is also the outcome of the wavelet decomposition of $g(p,q)$, the outcomes of a wavelet transform can be defined as:

$$\begin{cases} A(p,q) = g_C(p,q); \\ D_1(p,q) = g_C(p, q+\left[\frac{N}{2}\right]); \\ D_2(p,q) = g_C(p+\left[\frac{M}{2}\right], q); \\ D_3(p,q) = g_C(p+\left[\frac{M}{2}\right], q+\left[\frac{N}{2}\right]); \\ where\ 0 \le p \le \left[\frac{M}{2}\right] - 1, 0 \le q \le \left[\frac{N}{2}\right] - 1. \end{cases} \quad (4)$$

One level of wavelet decomposition generates one smooth sub-image and three detail sub-images that contain fine structures with horizontal, vertical, and diagonal orientations. An image is decomposed by wavelet transform into one approximation sub-image (A) and three detail sub-images (D_1, D_2 and D_3). These four sub-images, each of which has a size of (M/2 x N/2) pixels, form the wavelet characteristics. Wavelet transform provides a convenient way to obtain a multi-resolution representation, from which texture features can be easily extracted. The merits of using wavelet transform include local image processing, simple calculations, high speed processing and multiple image information [19-21].

2.2 Wavelet-based principal component analysis

Principal component analysis (PCA) is a popular technique for data compression and has been successfully used as initial step in many computer vision tasks [22-23]. The principal components of a set of process variables x_1, x_2, …, x_p are just a particular set of linear combinations of these variables. Geometrically, the principal component variables y_1, y_2, …, y_p are the axes of a new

ISSN: 1991-8755 Issue 4, Volume 3, April 2008

coordinate system obtained by rotating the axes of the original system (the *p*'s). The new axes represent the directions of maximum variability.

The basic intent of principal components is to find the new set of orthogonal directions that define the maximum variability in the original data, and this will lead to a description of the process requiring considerably fewer than the original *p* variables. The information contained in the complete set of all *p* principal components is exactly equivalent to the information in the complete set of all original process variables, but hopefully we can use far fewer than *p* principal components to obtain a satisfactory description [24].

The WPCA approach decomposes an image of size (*M* x *N*) pixels into a set of *a* x *b* multivariate processing units. Therefore, an original image has *g* x *h* (i.e. *M*/*a* x *N*/*b*) multivariate processing units. For each multivariate processing unit, the region of size *a* x *b* pixels can be applied the wavelet transform to obtain four wavelet characteristics *A*, D_1, D_2 and D_3 through calculations. The PCA integrates the multiple wavelet characteristics into a PC score for each multivariate processing unit. This PC score can be regarded as an distance value of a multivariate processing unit. The larger the PC score, the more the difference between the region and normal area. Therefore, this region can be judged as a defective region, otherwise this region has no defect.

Let the four random variables x_1, x_2, x_3, x_4 be the four wavelet characteristics and be represented by a vector $\boldsymbol{X} = [A, D_1, D_2, D_3]^T$ with covariance matrix $\boldsymbol{\Sigma}$, and let the eigenvalues of $\boldsymbol{\Sigma}$ be λ_1, λ_2, λ_3, λ_4. Then the constants e_{ij} are simply the elements of the *i*th eigenvector $\boldsymbol{e}_i$ associated with the eigenvalue λ_i. Basically, if we let $\boldsymbol{E}$ be the matrix whose columns are the eigenvectors, then

$$\boldsymbol{E}'\boldsymbol{\Sigma}\boldsymbol{E} = \boldsymbol{\Lambda} \tag{5}$$

where $\boldsymbol{\Lambda}$ is a 4 × 4 diagonal matrix with main diagonal elements equal to the eigenvalues $\lambda_1 \geq \lambda_2 \geq ... \geq \lambda_4 \geq 0$. More specifically, the equation can be expressed by the eigenvalues and the eigenvectors as follows:

$$[\boldsymbol{e}_1\ \boldsymbol{e}_2\ \boldsymbol{e}_3\ \boldsymbol{e}_4]\begin{bmatrix} \sigma_A^2 & \sigma_{A,D_1} & \sigma_{A,D_2} & \sigma_{A,D_3} \\ \sigma_{D_1,A} & \sigma_{D_1}^2 & \sigma_{D_1,D_2} & \sigma_{D_1,D_3} \\ \sigma_{D_2,A} & \sigma_{D_2,D_1} & \sigma_{D_2}^2 & \sigma_{D_2,D_3} \\ \sigma_{D_3,A} & \sigma_{D_3,D_1} & \sigma_{D_3,D_2} & \sigma_{D_3}^2 \end{bmatrix}\begin{bmatrix} \boldsymbol{e}_1 \\ \boldsymbol{e}_2 \\ \boldsymbol{e}_3 \\ \boldsymbol{e}_4 \end{bmatrix} = \begin{bmatrix} \lambda_1 & 0 & 0 & 0 \\ 0 & \lambda_2 & 0 & 0 \\ 0 & 0 & \lambda_3 & 0 \\ 0 & 0 & 0 & \lambda_4 \end{bmatrix} \tag{6}$$

The principal component analysis can be performed by computing the eignvalues and eignvectors [25].

The variance of the *i*th principal component is the *i*th eigenvalue λ_i. Consequently, the proportion of variability in the original data explained by the *i*th principal component is given by the ratio $\lambda_i/(\lambda_1+\lambda_2+\cdots+\lambda_4)$. Therefore, one can easily see how much variability (for instance, 80 to 90%) is explained by retaining just a few (say, *r*) of the 4 principal components simply by computing the sum of the eigenvalues for those *r* components and comparing that total to the sum of all 4 eigenvalues.

Once the principal components have been calculated and a subset of them selected, we can obtain new principal component observations y_{ij} (principal component (PC) scores) simply by substituting the original observations x_{ij} into the set of *r* retained principal components. After conducting many experiments, we find the first one principal component accounts for most of the variability in this study. If we have retained the first one (i.e. *r*=1) of the original four principal components, then the PC score $Y_{M(x,y)}$ of the multivariate processing unit $M(x,y)$ of a testing image can be defined as:

$$Y_{M(x,y)} = \left| e_1^T\left(X_{M(x,y)} - \bar{X}\right)\right| \tag{7}$$

where $X_{M(x,y)} = \begin{bmatrix} A(x,y) \\ D_1(x,y) \\ D_2(x,y) \\ D_3(x,y) \end{bmatrix}_{4\times 1}$, and

$\bar{X} = \begin{bmatrix} A^{\max} \\ D_1^{\min} \\ D_2^{\min} \\ D_3^{\min} \end{bmatrix}_{4\times 1}$, $A^{\max}$: maximum value of *A*s in a normal image; $D_1^{\min}$: minimum value of D_1s in a normal image; $D_2^{\min}$: minimum value of D_2s in a normal image; $D_3^{\min}$: minimum value of D_3s in a normal image

and $\boldsymbol{e}_1^T = [e_{11}, e_{12}, e_{13}, e_{14}]$ is the first eigenvector of the $\boldsymbol{\Sigma}$ of a testing image. Normal texture images are used to estimate the parameters of standard texture characteristics for bonding pad and emitting area, respectively. The sample expected matrix of the wavelet characteristics ($\bar{X}$) describes the properties and relations between normal and defect images. The threshold value (*T*) is defined as follows:

$$T = \bar{Y} + K\sigma_Y \tag{8}$$

where *K* is a constant empirically determined, $\bar{Y}$ and σ_Y are respectively the mean value and the

ISSN: 1991-8755 Issue 4, Volume 3, April 2008

standard deviation of the PC scores of a normal image. Therefore, if a multivariate processing unit $M(x, y)$ of a testing image $f(x, y)$ has a higher PC score, it implies that the region contains defects in the testing image. On the contrary, a lower PC score signifies that no defect exist in the corresponding region of the image.

2.3 Wavelet-based Hotelling statistic method

The wavelet-based Hotelling statistic (WHS) method decomposes an image of (M x N) pixels into a set of sub-images, each of which has a size of (m x n) pixels and is a multivariate processing unit. The original image has g x h (i.e. M/m x N/n) multivariate processing units, each of which can be further decomposed into a x b wavelet processing units. For each wavelet processing unit, the wavelet transform can be applied to the region of (m/a x n/b) pixels to obtain four wavelet characteristics A, D_1, D_2 and D_3 through calculations. The Hotelling statistic T^2 integrates the multiple wavelet characteristics into a T^2 value for each multivariate processing unit. This T^2 value can be regarded as a distance value of a multivariate processing unit. The larger the T^2 statistic value, the more distinctive the region is from the normal area. Thus, the more easily the region can be judged as defective.

The proposed WHS approach assumes that the size of a multivariate processing unit is 4 x 4 (i.e. m x n) pixels and the size of a wavelet processing unit is 2 x 2 (i.e. a x b) pixels. One multivariate processing unit will have 2 x 2 (i.e. m/a x n/b) wavelet processing units. That is, four wavelet processing units $C(x_a, y_b)$ can be defined as one multivariate processing unit $M(x, y)$, where a and b are integers and $(1 \leqq a,\ b \leqq 2)$. The corresponding spatial coordinates of $C(x_a, y_b)$ are a square with size 2 x 2 pixels from $f(4\times x+k, 4\times y+l)$ to $f(4\times x+k+1, 4\times y+l+1)$. Thus, one $M(x, y)$ includes four $C(x_a, y_b)$, which are $C(x_1, y_1)$, $C(x_1, y_2)$, $C(x_2, y_1)$ and $C(x_2, y_2)$. One $C(x_a, y_b)$ can be decomposed by wavelet transform to obtain one approximated characteristic $A(x_a, y_b)$ and three detail characteristics $D_1(x_a, y_b)$, $D_2(x_a, y_b)$ and $D_3(x_a, y_b)$.

The calculation formulas of a multivariate control procedure [26-27] can be rewritten as Eqs. (9) to (14) to represent a multivariate process of images.

$$\overline{X}_{M(x,y)} = \left[\frac{1}{a\times b} \sum_{i=1}^{a} \sum_{j=1}^{b} X_{C(x_i, y_j), p} \right]_{p\times 1} \tag{9}$$

$$\overline{\overline{X}} = \left[\frac{1}{g\times h} \sum_{i=0}^{g-1} \sum_{j=0}^{h-1} \overline{X}_{M(i,j),p} \right]_{p\times 1} \tag{10}$$

$$S^2_{M(x,y),p} = \frac{1}{a\times b-1} \sum_{i=1}^{a} \sum_{j=1}^{b} \left(X_{C(x_i, y_j), p} - \overline{X}_{M(x,y),p} \right)^2 \tag{11}$$

$$S_{M(x,y),p,q} = \frac{1}{a\times b-1} \sum_{i=1}^{a} \sum_{j=1}^{b} \left(X_{C(x_i, y_j), p} - \overline{X}_{M(x,y),p} \right) \left(X_{C(x_i, y_j), q} - \overline{X}_{M(x,y),q} \right) \tag{12}$$

$$S^2_p = \frac{1}{g\times h} \sum_{i=0}^{g-1} \sum_{j=0}^{h-1} S^2_{M(i,j),p} \tag{13}$$

$$S_{p,q} = \frac{1}{g\times h} \sum_{i=0}^{g-1} \sum_{j=0}^{h-1} S_{M(i,j),p,q} \tag{14}$$

where $X_{C(x_a, y_b), p}$ is the p-th image characteristic of a wavelet processing unit $C(x_a, y_b)$; $\overline{X}_{M(x,y)}$ is the mean matrix of image characteristics in a multivariate processing unit $M(x, y)$; $\overline{X}_{M(i,j),p}$ is the mean value of the p-th image characteristic of $M(i, j)$; $S^2_{M(x,y),p}$ is the variance of the p-th image characteristic of $M(x, y)$; $S_{M(x,y),p,q}$ is the covariance of the p-th and the q-th image characteristics of $M(x, y)$. The multivariate matrices used in this research can be expressed as follows:

$$X_{C(x_a, y_b)} = \begin{bmatrix} A(x_a, y_b) \\ D_1(x_a, y_b) \\ D_2(x_a, y_b) \\ D_3(x_a, y_b) \end{bmatrix} \tag{15}$$

$$\bar{X}_{M(x,y)} = \begin{bmatrix} \bar{A}(x,y) \\ \bar{D}_1(x,y) \\ \bar{D}_2(x,y) \\ \bar{D}_3(x,y) \end{bmatrix}_{4\times 1} = \begin{bmatrix} \frac{1}{a\times b} \sum_{i=1}^{a} \sum_{j=1}^{b} A(x_i, y_j) \\ \frac{1}{a\times b} \sum_{i=1}^{a} \sum_{j=1}^{b} D_1(x_i, y_j) \\ \frac{1}{a\times b} \sum_{i=1}^{a} \sum_{j=1}^{b} D_2(x_i, y_j) \\ \frac{1}{a\times b} \sum_{i=1}^{a} \sum_{j=1}^{b} D_3(x_i, y_j) \end{bmatrix}_{4\times 1} \tag{16}$$

Normal texture images are used to estimate the parameters of standard texture characteristics. The sample mean matrix (a x b) and the sample covariance matrix (S) describe the properties and relations between normal and defect images. The $\overline{\overline{X}}$ and S are defined as:

ISSN: 1991-8755 Issue 4, Volume 3, April 2008

$$\overline{\overline{X}} = \begin{bmatrix} \overline{\overline{A}} \\ \overline{\overline{D}}_1 \\ \overline{\overline{D}}_2 \\ \overline{\overline{D}}_3 \end{bmatrix}_{4\times 1} \tag{17}$$

$$S = \begin{bmatrix} S_A^2 & S_{A,D_1} & S_{A,D_2} & S_{A,D_3} \\ S_{D_1,A} & S_{D_1}^2 & S_{D_1,D_2} & S_{D_1,D_3} \\ S_{D_2,A} & S_{D_2,D_1} & S_{D2}^2 & S_{D_2,D_3} \\ S_{D_3,A} & S_{D_3,D_1} & S_{D_3,D_2} & S_{D_3}^2 \end{bmatrix}_{4\times 4} \tag{18}$$

where S_p^2 is the sample variance of the *p*-th wavelet characteristic of an image; $S_{p,q}$ is the sample covariance of the *p*-th and the *q*-th wavelet characteristics of an image.

The T^2 statistic value of the multivariate processing unit $M(x,y)$ of a testing image can be defined as:

$$T^2_{M(x,y)} = a \times b \left[\overline{X}_{M(x,y)} - \overline{\overline{X}} \right]^T S^{-1} \left[\overline{M}_{M(x,y)} - \overline{\overline{X}} \right] \tag{19}$$

where *a x b* is the number of wavelet process units in a multivariate processing unit. $\overline{X}_{M(x,y)}$ is the mean matrix of image characteristics in the multivariate processing unit of a testing image. The $\overline{\overline{X}}$ and *S* are respectively the mean matrix and the covariance matrix of image characteristics of a normal image. The upper control limit is as follows:

$$\frac{p(m-1)(n-1)}{mn-m-p+1} F_{\theta,p,(mn-m-p+1)} \tag{20}$$

,where *F* is a tabulated value of the *F* distribution at the significance level of θ.

3 Experiments and Analyses

To evaluate the performance of the proposed approaches, experiments are conducted on real LED chips provided by a company that manufactures high quality LED chips in Taiwan. We test 180 LED chip images, of which 60 have no defects and 120 have various water-spot defects. All of the samples are randomly selected from the manufacturing process of LED chips. All experiments are implemented on a Pentium IV personal computer with 2.6GHz CPU and 512 MB RAM; and all programming is done in the C language.

To increase the number of LED chips on a wafer, every chip is located very close to its neighboring chips. As the carrier plate moves to have the image of the next chip captured, the movement might cause the CCD to deviate from its original position and the image capturing device to vibrate. Thus, the images of all the chips might be captured with slight differences. That is, not all the chips are located in the exactly same positions in their individual images. As a result, two areas are needed for each image to specify the locations of two different background textures in which water-spot defects may possibly exist. The LED emitting area and bonding pad need to be separated first and then individually apply the proposed methods to detect defects.

In the outer area of an LED chip is an emitting area which contains uniform texture. Since wavelet transform can process images of rectangular shapes, a specially made background must be added to convert the different shape region into a rectangular one. Thus, we change gray levels of the area falling outside the outer area to the average gray level of normal chip images in Fig. 3(a). With such a manipulated background, we not only obtain a rectangular region for wavelet transform but also minimize the affect non-emitting region. Once the mixed image is transformed into the wavelet domain, the non-emitting region will not interfere in the feature extraction of the emitting region.

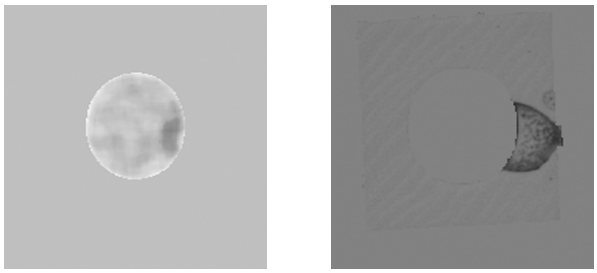

(a) (b)

Fig. 3 The mixed images (a) for the bonding pad (b) for the emitting area

Similarly, this procedure is also applied to defect detection on LED bonding pad except additionally taking median filtering operation. In the central area of an LED chip is a bonding pad which contains statistical texture with random particles like pepper noises. The more similar the gray levels of the particles on bonding pad and the water-spot defect, the more difficult it is to distinguish the defect and the random particles. The median filter [29] is used to smooth the particles on the random texture. The mask

ISSN: 1991-8755 Issue 4, Volume 3, April 2008

of size 11 x 11 pixels is capable of smoothing all the random particles in the testing samples, as shown in Fig. 3 (b). Then, the filtered images are conducted the gray level changes of the area falling outside the central area for the same purpose described in Fig. 3 (a).

For the proposed WPCA and WHS approaches, we found the most appropriate sizes of multivariate processing units to be 2 x 2 and 4 x 4 pixels, respectively, after conducting various experiments. At these sizes, the two methods achieve the best performance considering the sample training time, the recognition time of the testing period, the size of the defect area and other factors in the multivariate processing.

To verify the performance of the proposed methods, we compare the results of our experiments against those provided by professional inspectors. Figure 4 shows partial results of detecting water-spot defects (Fig. 2 (b)-(d)) by the Otsu method [29], the proposed WHS and WPCA approaches, and the professional inspector, individually. The WHS and WPCA methods detect most of the water-spot blemishes while the Otsu method misses some defect regions.

The performance evaluation indices, *(1-α)* and *(1-β)*, are used to represent correct detection judgments; the higher the two indices, the more accurate the detection results. Statistical type I error α suggests the probability of producing false alarms, i.e. detecting normal regions as defects. Statistical type II error β implies the probability of producing missing alarms, which fail to alarm real defects. We divide the area of normal region detected as defects by the area of actual normal region to obtain type I error, and the area of undetected defects by the area of actual defects to obtain type II error. The correct classification rate (CR) is defined as:

$$CR = (N_{cc} + N_{dd}) / N_{total} \times 100\% \quad (21)$$

where N_{cc} is the pixel number of normal textures detected as normal areas, N_{dd} is the pixel number of ripple defects detected as defective regions, and N_{total} is the total pixel number of a testing image.

The average detection rates *(1-β)* of all testing samples by the three methods are, respectively, 86.6% (Otsu method), 91.3% (WHS method), and 93.8% (WPCA method). The average false alarm rates *(α)* of all testing samples are, respectively, 9.3% (Otsu method), 5.8% (WHS method), and 3.6% (WPCA method). The proposed wavelet based multivariate statistical approaches have higher detection rates *(1-β)* and correct classification rates

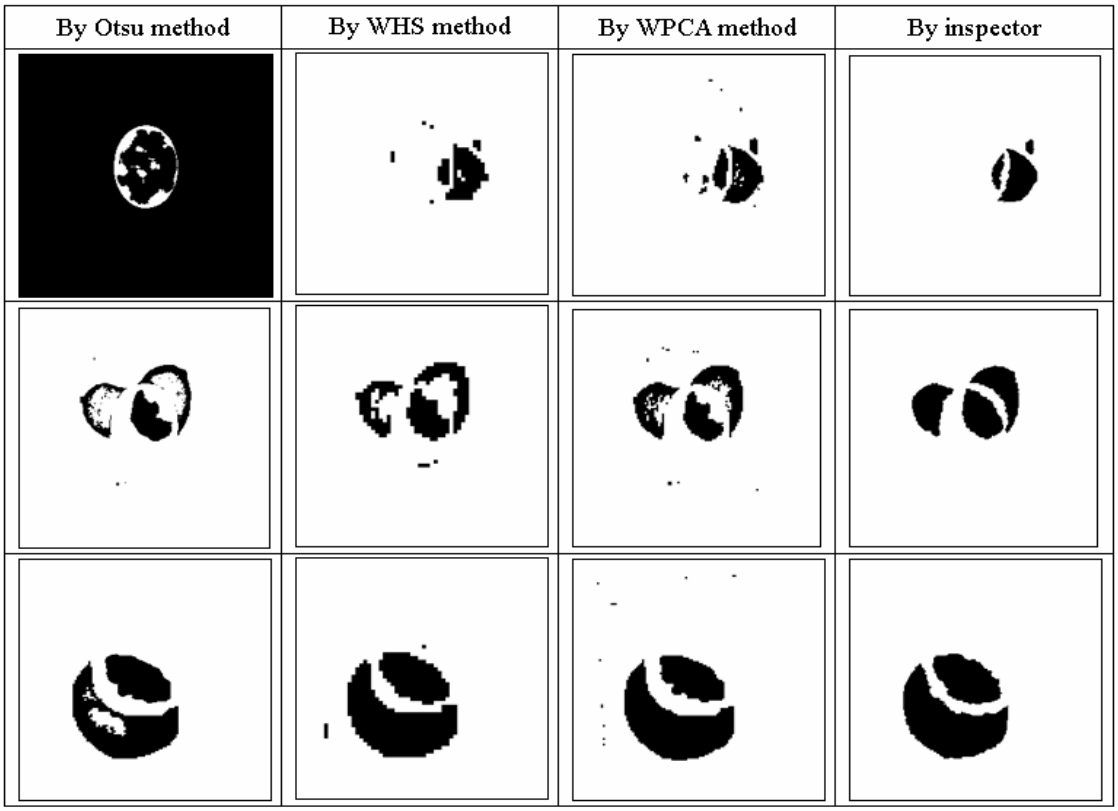

Fig. 4 Partial detection results of the Otsu, WHS, WPCA, and the professional inspector

ISSN: 1991-8755 Issue 4, Volume 3, April 2008

(CR) than does the traditional method applied to LED chip images. The WPCA method not only excels in its ability of correctly discriminating water-spot defects from normal regions but also has the lowest false alarm rate. The average computation time for processing an image of 256 x 256 pixels is as follows: 1.84 seconds (Otsu method), 2.32 seconds (WHS method), and 2.26 seconds (WPCA method). Both of the multivariate statistical approaches based on the wavelet characteristics have the same processing time.

As the decision threshold value changes, so do its false alarm rate (α) and detection rate (1- β), both of which are used to describe the performance of a test according to hypothesis testing theory [30]. When various decision thresholds (Eqs. (8) and (20)) are used, their pairs of false alarm rates and detection rates are plotted as points on a Receiver Operating Characteristic (ROC) curve. Figures 5 and 6 present the two ROC curves of the WHS and WPCA approaches, and the one point of the Otsu method for the bonding pad and the emitting area respectively. The upper-left corners of Figs. 5 and 6 are the optimum points, which have a 100% detection rate and a 0% false alarm rate. The more the ROC plot approaches the upper-left corner, the better the test performs. In industrial practices, a more than 90% defect detection rate and a less than 10% false alarm rate are a good rule of thumb for performance evaluation of a vision system. Accordingly, the proposed WPCA approach, with its ROC plots closer to the upper-left corner, outperforms the WHS method and the traditional Otsu method.

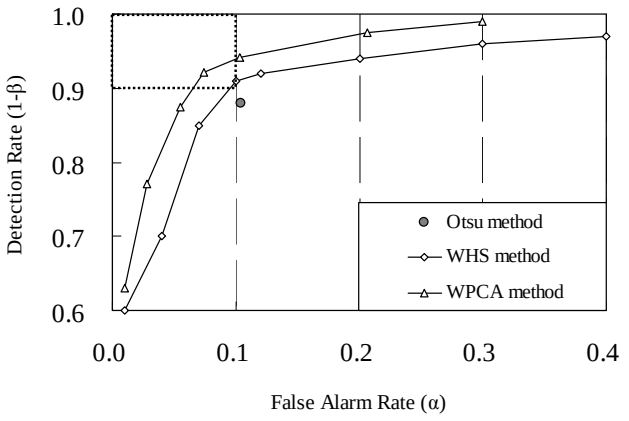

Fig. 5 ROC plots of the Otsu, WHS, and WPCA methods for the bonding pad

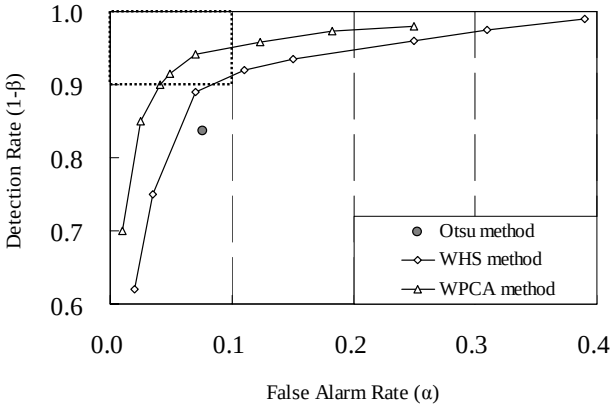

Fig. 6 ROC plots of the Otsu, WHS, and MPCA methods for the emitting area

The WPCA approach achieves good performance in detecting surface defects of LED chips as well as semi-opaque and low-intensity-contrast water-drop blemishes that fall across two different background textures. Since the computation of multivariate statistics is based on the mean vector and covariance matrix of the training samples, lighting changes may lead to an increase of variation in statistics and result in a decline of defect detection performance. Thus, it is recommended to re-compute the mean vector and covariance of the training samples whenever illumination is significantly changed. In addition, the proposed method is not recommended for detecting blemishes embedded in structural textures because it is designed to identify defects in random textures.

4 Conclusion

Machine vision technology improves productivity and quality management, and provides a competitive advantage to industries that employ this technology. This research applies wavelet-based multivariate statistical approaches combined with machine vision techniques to detect water-spot blemishes that fall across two different background textures of LED chips. The research methods use the principal component analysis and Hotelling statistic, respectively, based on wavelet characteristics to judge the existence of water-spot defects through multivariate processes of combining image characteristics from wavelet decomposition of local image blocks.

Experimental results show that the WPCA approach achieves detection rates of above 93.8% and false alarm rates of below 3.6% in detecting water-spot blemishes across two different background textures. As indicated in the ROC curve analysis, the WPCA approach has better defect

ISSN: 1991-8755 Issue 4, Volume 3, April 2008

detection rates and lower false alarm rates than do the WHS and Otsu methods. This research contributes a solution to a common surface defect detection problem of LED chips and offers a computer-aided visual defect inspection system to meet the inspection and quality control request.

Acknowledgements:
The authors thank the National Science Council of Taiwan (R.O.C.) for the financial support through the Grant NSC 95-2221-E-324-034-MY2.

References:

[1] Wang, Z., Ji, S., Zhang, L., Huan,Y., and Yang G., Research on automatic detecting technology of Razor's assembling quality based on the machine vision system, *WSEAS Transactions on Computers*, Vol.5, No.6, 2006, pp.1319-1324.

[2] Furferi, R. and Governi, L., Development of an artificial vision inspection system for real-time defect detection and classification on circular knitting machines, *WSEAS Transactions on Computers*, Vol.5, No.6, 2006, pp.1186-1193.

[3] Zhong, Z.W. and Shankar, N.G., A clustering technique for defect inspection, *WSEAS Transactions on Electronics*, Vol.2, No.4, 2005, pp.185-188.

[4] Malamas, E.N., Petrakis, E.G.M, Zervakis, M., Petit, L., and Legat, J.D., A survey on industrial vision systems, applications and tools, *Image and Vision Computing*, Vol.21, 2003, pp.171-188.

[5] Kumar, A., Neural network based detection of local textile defects, *Pattern Recognition*, Vol.36, 2003, pp.1645-1659.

[6] Lin, H.D., Computer-aided visual inspection of surface defects in ceramic capacitor chips, *Journal of Materials Processing Technology*, Vol.189, No.1-3, 2007, pp.19-25.

[7] Huang, C.J., Clustered defect detection of high quality chips using self-supervised multilayer perceptron, *Expert Systems with Applications*, Vol.33, 2007, pp.996-1003.

[8] Siew, L.H., Hodgson, R.M., and Wee, L.K., Texture measures for carpet wear assessment, *IEEE Transactions on Pattern Analysis and Machine Intelligence*, Vol.10, 1988, pp.92-150.

[9] Latif-Amet, A., Ertüzün, A., and Ercil, A., An efficient method for texture defect detection: sub-band domain co-occurrence matrices, *Image and Vision Computing*, Vol.18, 2000, pp.543-553.

[10] Chan, C.H. and Pang, G.K.H., Fabric defect detection by Fourier analysis, *IEEE Transactions on Industrial Applications*, Vol.36, No.5, 2000, pp.1267-1276.

[11] Kumar, A. and Pang, G.K.H., Defect detection in textured materials using Gabor filters, *IEEE Transactions on Industrial Applications*, Vol.38, No.2, 2002, pp.425-440.

[12] Lin, H.D., Tiny surface defect inspection of electronic passive components using Discrete Cosine Transform decomposition and cumulative sum techniques, *Image and Vision Computing*, Vol.26, No.5, 2008, pp.603-621.

[13] Lin, H.D. and Chiu, S.W., Computer-aided vision system for MURA-type defect inspection in liquid crystal displays, *Lecture Notes in Computer Science*, Vol.4319, 2006, pp.442-452.

[14] Lu, C.J. and Tsai, D.M., Defect inspection of patterned TFT-LCD panels using a fast sub-image based SVD, *International Journal of Production Research*, Vol.42, 2004, pp.4331-4351.

[15] Maruo, K., Shibata, T., Yamaguchi, T., Ichikawa, M., and Ohmi, T., Automatic defect pattern detection on LSI wafers using image processing techniques, *IEICE Transactions on Electronics*, Vol.82, 1999, pp.1003-1012.

[16] Shankar, N.G. and Zhong, Z.W., Defect detection on semiconductor wafer surfaces, *Microelectronic Engineering*, Vol.77, 2005, pp.337-346.

[17] Lin, H.D. and Ho, D.C., Detection of pinhole defects on chips and wafers using DCT enhancement in computer vision systems, *International Journal of Advanced Manufacturing Technology*, Vol.34, No.5-6, 2007, pp.567-583.

[18] Fadzil, M.H.A. and Weng, C.J., LED cosmetic flaw vision inspection system, *Pattern Analysis & Application*, Vol.1, 1998, pp.62-70.

[19] Gonzalez, R.C. and Woods, R.E., *Digital Image Processing*, 2nd edn., Prentice-Hall, Upper Saddle River, NJ, 2002, pp.349-403.

[20] Arivazhagan, S. and Ganesan, L., Texture segmentation using wavelet transform, *Pattern Recognition Letters*, Vol.24, 2003, pp.3197-3203.

[21] Bashar, M.K., Matsumoto, T., and Ohnishi, N., Wavelet transform-based locally orderless images for texture segmentation, *Pattern Recognition Letters*, Vol.24, 2003, pp.2633-2650.

[22] Mirapeix, J., Garcia-Allende, P.B., Cobo, A., Conde, O.M., and Lopez-Higuera, J.M., Real-time arc-welding defect detection and classification with principal component analysis and artificial neural networks, *NDT & E International*, Vol.40, No.4, 2007, pp.315-323.

[23] Thomaz, C.E., Boardman, J.P., Counsell, S., Hill, D.L.G., Hajnal, J.V., Edwards, A.D., Rutherford, M.A., Gillies, D.F., and Rueckert, D., A multivariate statistical analysis of the developing human brain in preterm infants, *Image and Vision Computing*, Vol.25, 2007, pp.981-994.

[24] Montgomery, D.C., *Introduction to Statistical Quality Control*, 5th edn, John Wiley & Sons, Hoboken, NJ, 2005, pp.491-504.

[25] Johnson, R.A. and Wichern, D.W., *Applied Multivariate Statistical Analysis*, 5th edition, Prentice-Hall, Inc., Upper Saddle River, NJ, 2002, pp.426-437.

[26] Hotelling, H., Multivariate quality control, in: Eisenhart C, Hastay M W & Wallis W A (Eds.), *Techniques of Statistical Analysis*, McGraw-Hill, New York, NY, 1947, pp.111-184.

[27] Lowry, C.A. and Montgomery, D.C., A review of multivariate control charts, *IIE Transactions*, Vol.27, 1995, pp.800-810.

[28] Jain, R., Kasturi, R., and Schunck, B.G., *Machine Vision*, International edn, McGRAW-Hill, New York, NY, 1995, pp.80-83.

[29] Otsu, N., A threshold selection method from gray-level histogram, *IEEE Transactions on Systems, Man, Cybernetics*, Vol.9, 1979, pp.62-66.

[30] Montgomery, D.C. and Runger, G.C., *Applied Statistics and Probability for Engineers*, 2th edn, John Wiley & Sons, New York, NY, 1999, pp.296-304.